EUROPEAN SYNCHROTRON RADIATION FACILITY

INSTALLATION EUROPEENNE DE RAYONNEMENT SYNCHROTRON

ESRF

Experiment Report Form

The double page inside this form is to be filled in by all users or groups of users who have had access to beam time for measurements at the ESRF.

Once completed, the report should be submitted electronically to the User Office via the User Portal:
https://wwws.esrf.fr/misapps/SMISWebClient/protected/welcome.do

Deadlines for submission of Experimental Reports

Experimental reports must be submitted within the period of 3 months after the end of the experiment.

Experiment Report supporting a new proposal ("relevant report")

If you are submitting a proposal for a new project, or to continue a project for which you have previously been allocated beam time, you must submit a report on each of your previous measurement(s):

- even on those carried out close to the proposal submission deadline (it can be a *"preliminary report"),*
- even for experiments whose scientific area is different form the scientific area of the new proposal,
- carried out on CRG beamlines.

You must then register the report(s) as "relevant report(s)" in the new application form for beam time.

Deadlines for submitting a report supporting a new proposal

- 1st March Proposal Round - **5th March**
- 10th September Proposal Round - **13th September**

The Review Committees reserve the right to reject new proposals from groups who have not reported on the use of beam time allocated previously.

Reports on experiments relating to long term projects

Proposers awarded beam time for a long term project are required to submit an interim report at the end of each year, irrespective of the number of shifts of beam time they have used.

Published papers

All users must give proper credit to ESRF staff members and proper mention to ESRF facilities which were essential for the results described in any ensuing publication. Further, they are obliged to send to the Joint ESRF/ ILL library the complete reference and the abstract of all papers appearing in print, and resulting from the use of the ESRF.

Should you wish to make more general comments on the experiment, please note them on the User Evaluation Form, and send both the Report and the Evaluation Form to the User Office.

Instructions for preparing your Report

- fill in a separate form for each project or series of measurements.
- type your report in English.
- include the experiment number to which the report refers.
- make sure that the text, tables and figures fit into the space available.
- if your work is published or is in press, you may prefer to paste in the abstract, and add full reference details. If the abstract is in a language other than English, please include an English translation.

ESRF	**Experiment title:** Multiscale structure – performance relations in printed polymeric materials	**Experiment number**: A26-2-962
Beamline: BM 26	**Date of experiment**: from: 6th May 2023 to: 13th May 2023	**Date of report**:
Shifts: 18	**Local contact(s)**: Martine Rosenthal	*Received at ESRF:*

Names and affiliations of applicants (* indicates experimentalists):

***Francisco Molina-Lopez (Department of Materials Engineering (MTM), KU Leuven, Belgium)**

***Tzu-Yi Yu (Department of Materials Engineering (MTM), KU Leuven, Belgium)**

***Tsu-Yu Chou (Department of Materials Engineering (MTM), KU Leuven, Belgium)**

***Hasan Emre Baysal (Department of Materials Engineering (MTM), KU Leuven, Belgium)**

***Viktor Naenan (Department of Materials Engineering (MTM), KU Leuven, Belgium)**

***Tanmay Sinha (Department of Materials Engineering (MTM), KU Leuven, Belgium)**

ESRF experiment report

Beamline: BM26

Project: CRG – DUBBLE

Experiment time: 6th – 13th May 2023

Main proposer:

- **Francisco Molina-Lopez** (Department of Materials Engineering (MTM), KU Leuven, Belgium)

Participant:

- **Francisco Molina-Lopez** (Department of Materials Engineering (MTM), KU Leuven, Belgium)
- **Tzu-Yi Yu** (Department of Materials Engineering (MTM), KU Leuven, Belgium)
- **Hasan Emre Baysal** (Department of Materials Engineering (MTM), KU Leuven, Belgium)
- **Tanmay Sinha** (Department of Materials Engineering (MTM), KU Leuven, Belgium)
- **Tsu-Yu Chou** (Department of Materials Engineering (MTM), KU Leuven, Belgium)
- **Viktor Naenan** (Department of Materials Engineering (MTM), KU Leuven, Belgium)

Local contact:

- **Martin Rosenthal**

Introduction

Wearable devices are compact, lightweight, and usually mechanically flexible. However, the power supply and storage of wearable devices are the bottleneck to their development. Organic-based thermoelectrics (OTEs) and photovoltaics (OPVs) are promising solutions to supply power, but their energy-harvesting efficiencies are still far from the need for powering wearable devices. Since the electrical properties of organic materials are strongly bonded to their crystalline microstructure, the structural characterization and its correlation to material properties are key to enhancing the performance of OTEs and OPVs.

The two main factors defining thermoelectric performance - electrical conductivity and the Seebeck coefficient - are both a function of carrier concentration but with opposite correlation (electrical conductivity increases with charge carrier concentration and Seebeck decreases). To enhance the OTEs performance, the typical strategy is to tune the amount of dopants (oxidants) or reductants to optimize the carrier concentration.[1,2] This trade-off relation limits the maximum thermoelectric power output. In contrast to oxidants and reductants, some additives can synergistically enhance both factors. [3] Rather than strongly changing the doping level, these additives modify the crystalline microstructure of the conducting polymer used as OTE, and improve the carrier mobility. Such morphology modifiers, also called secondary dopants, break the thermoelectric power output limitation imposed by the abovementioned charge carrier density trade-off. To power wearable devices, our PEDOT:PSS-based OTEs materials are designed to be printable and mechanically flexible. Besides improving performance, some additives can work as plasticizers, helping to achieve the desired mechanical properties[4] To precisely optimize the additive composition for the desired mechanical and thermoelectric properties, an essential aspect is to identify the role of each additive. X-ray scattering offers detailed microstructural information to know if a certain additive is an efficient morphology modifier (secondary dopant) or not.

As to organic photovoltaics, the active layer morphology is critical to harvest light efficiently. The photovoltaic effect takes place via a series of steps: absorption of photons leading to the formation of excitons, diffusion of excitons to interfaces between the donor and the acceptor, splitting of excitons

into electrons and holes, and transport of charge carriers to the respective electrodes. During the photoconversion process, electron-hole recombination causes conversion efficiency loss. The efficiency loss can be prevented by the fast transportation of carriers to electrodes, which relies on carrier mobility in the active layer. Since carrier mobility benefits from the crystalline phase of conducting polymer, OPVs efficiency can be boosted by enhancing the crystallinity and size of crystals with processing parameters. Therefore, the microstructural information from X-ray scattering studies is central to OPVs research.

The crystalline structure of conducting polymers is crucial to both OTEs and OPVs performance. During this beam time, x-ray scattering was utilized to investigate the microstructure of printed OTEs and OPVs materials. The microstructural changes resulting from tuning 1) the material composition and postprocessing of printed OTEs and 2) the processing conditions of printed OPVs materials were studied. The X-ray scattering results reveal the effect of the mentioned parameters, and guide a way to boost device performance by optimizing additive composition and processing parameters in printed OTEs and OPVs, respectively.

Experimental methods

During this beam time, two types of materials were characterized: 1) OTE bulk materials produced by direct-ink-writing (DIW); and 2) OPV thin films produced by ink-jet printing supported by a Silicon substrate. The OTE bulk materials are characterized by small-angle and wide-angle X-ray scattering (SAXS/WAXS), and the thin films are tested by grazing incident small-angle and wide-angle X-ray scattering (GISAXS/GIWAXS). All the data were collected by a Pilatus 1M detector with a 12 keV X-ray. The details of the data processing are described in the results and discussion sections.

Results and discussion

- **3D-printed (DIW) OTE**

In the present report, wide-angle x-ray scattering (WAXS) was utilized to study how additive and post-treatment affect the crystalline structure of printed PEDOT:PSS pillars. The pillar samples were printed by direct-ink-writing (DIW) PEDOT:PSS pastes with two additives, Li salt and (3-glycidyloxypropyl)trimethoxysilane (GOPS). Though the main purpose of the additives was enhancing the mechanical flexibility of printed PEDOT:PSS, these additives were also found to affect the thermoelectric properties of the resulting parts. Besides, post-treatment plays a role in improving the thermoelectric performance of printed pillars. Therefore, this WAXS experiment aims to connect material thermoelectric properties with additive amounts and post-treatment by studying the PEDOT crystalline microstructure of DIW printed pillars.

Peak intensity and position of PEDOT:PSS reflect the microstructural change from additives. The 1D linecut WAXS result of printed PEDOT:PSS pillars without (pristine) and with additives (w/ additives) are shown in **Figure 1**. Because each sample is assumed to contain the same ratio of PSS, the WAXS result are normalized by the PSS intensity. Two characteristic peaks in WAXS can be observed for the pristine sample; one broad peak centered around q = 1.2 $Å^{-1}$ represents the PSS π-π stacking, and another broad peak located at q = 1.8 $Å^{-1}$ represents the PEDOT π-π interchain stacking. These two peaks are also observed in the sample with Li salt and GOPS; however, the PSS peak shifts to a lower q value, while the PEDOT peak slightly shifts to a higher q value, and its intensity slightly decreases compared to the pristine sample. These changes indicate that additives affect the PSS structure and lower the PEDOT crystallinity (but meanwhile making PEDOT crystal more compact).

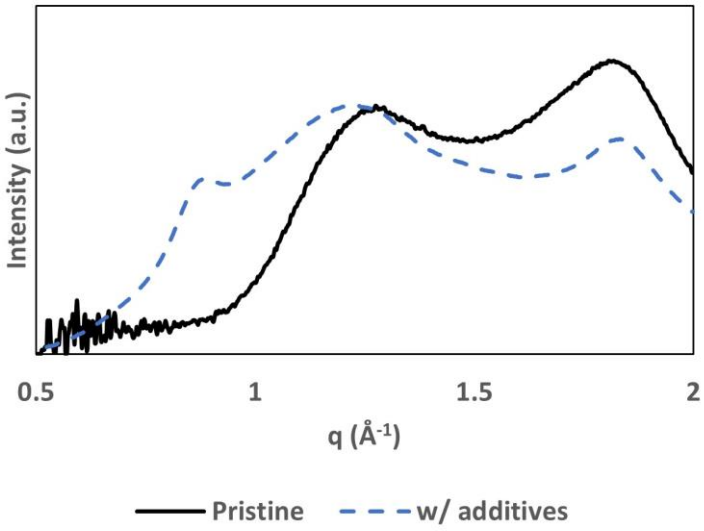

Figure 1. WAXS line intensity of printed PEDOT:PSS pillars prepared by pristine paste (–) and additives-containing paste (- -), respectively. The peak around q = 1.2 $Å^{-1}$ represents PSS π-π stacking and the one around q = 1.8 $Å^{-1}$ represents PEDOT π-π stacking.

Adding Li salt results in a fundamental change in PEDOT crystalline structure. Besides the two peaks credited to PSS and PEDOT π-π stacking, another peak was found around q = 0.9 $Å^{-1}$ in the WAXS pattern for additives-containing PEDOT:PSS pillars, (**Figure 1**). This peak presents a periodic structure with a spacing of about 7 Å, assigned as a PEDOT:PSS structure without a clear index in the literature. [4] According to the strong correlation between peak intensity and the amount of Li salt added in samples, as shown in **Figure 2(a)**, this peak should be accounted for the Li salt. Though the precise crystal structure after Li salt addition is not clear, the microstructural change from Li salt indicates its role as a morphology modifier to PEDOT:PSS.

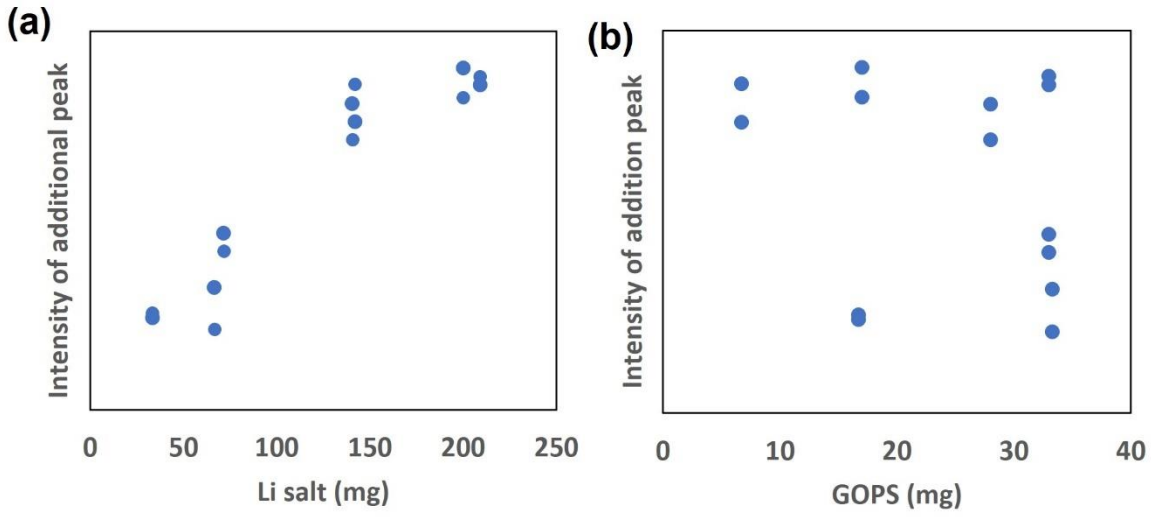

Figure 2. (a) Intensity of additional peak of samples containing varied amounts of Li salt additive. (b) Intensity of additional peak of samples containing varied amounts of GOPS additive.

In contrast to Li salt, GOPS is not related to the microstructural change of PEDOT:PSS. For instance, no correlation between GOPS content and the intensity of the scattering peak at q = 0.9 $Å^{-1}$ was found, as shown in **Figure 2(b).** The peak position and intensity of the other scattering peaks were

not affected by GOPS neither. Thus, the WAXS results suggest that GOPS is not considered a morphology modifier to PEDOT:PSS.

Li salt improves the electrical conductivity of PEDOT:PSS by forming compact PEDOT crystals. In the WAXS result, the peak around q = 1.8 $Å^{-1}$, which stands for PEDOT π-π stacking, shifts to a high q value in the sample containing Li salt, as shown in **Figure 3**. The peak shift has a positive correlation to the Li salt amount. Also, a positive correlation was found between PEDOT π-π spacing and electrical conductivity. This makes sense because a larger q value stands for a crystal structure with a closer π-π stacking distance that promotes transport. Thus, the role of Li salt as a morphology modifier, which enhances the thermoelectric performance of PEDOT:PSS, is confirmed.

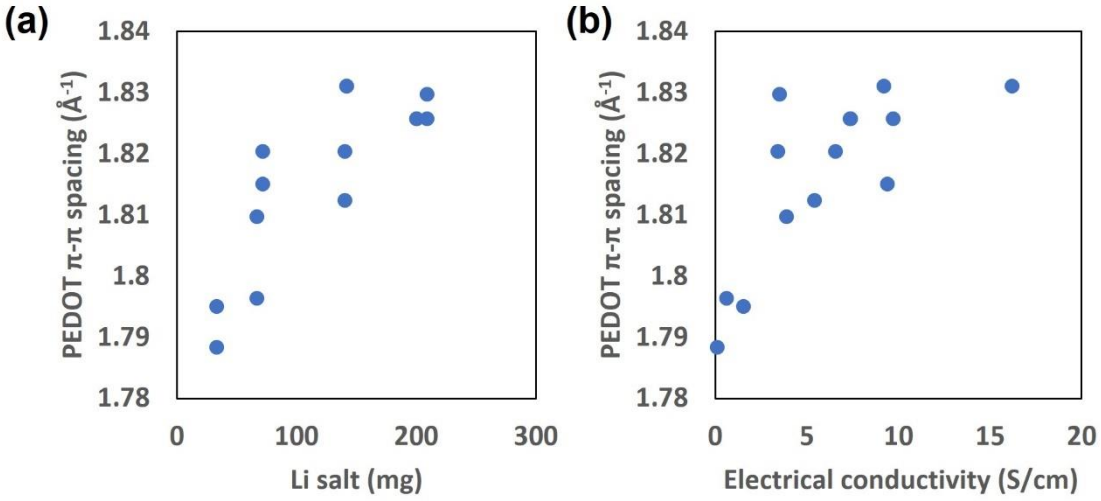

Figure 3. (a) PEDOT π-π spacing of samples containing varied amounts of Li salt additive. (b) correlation between PEDOT π-π spacing and electrical conductivity of samples.

The post-treatment effect is also studied in this WAXS experiment, but no structural difference from post-treatment was observed. In WAXS results, no significant change in the number, position, and intensity of peaks is found after treating PEDOT:PSS samples with ethanol vapor. The results suggest that the post-treatment doesn't change the microstructure of PEDOT:PSS at the nanometer scale. However, the enhancement in both electrical conductivity and Seebeck coefficient is observed after solvent vapor treatment, implying that post-treatment might change the microstructure of PEDOT:PSS at a larger scale (such as the sub-micrometer level). Therefore, other characterization techniques will help study the structural change from ethanol vapor post-treatment.

- **Ink-jet printed OPV**

The donor polymer PM6 and the small molecule acceptor Y6 have been shown to be an efficient system for OPVs, reaching a power conversion efficiency (PCE) as high as 28.8% under indoor light illumination [5]. The purpose of our study is to inkjet print a bulk heterojunction thin film active layer composed of these molecules for applications on smart wearables. The morphology of this layer is expected to be affected by a number of parameters, such as ink composition, plate temperature while printing, temperature of the cartridge nozzles, and post-thermal annealing temperature. The purpose of our visit to ESRF was to study how these parameters affect morphology. The samples prepared to do so have been listed in **Table 1** (spin coating is used as a reference process).

Table 1: List of Samples for GIWAXS measurements

Polymers	Solvents	Concentration	Plate temperature	Nozzle temperature	Annealing temperature	Method
PM6:Y6 (1:1.2)	o-xylene + 5v% tetralin	3 mg/ml	RT	RT	NA	Inkjet Printing
PM6:Y6 (1:1.2)	o-xylene + 5v% tetralin	3 mg/ml	RT	RT	165°C	Inkjet Printing
PM6:Y6 (1:1.2)	o-xylene + 5v% tetralin	3 mg/ml	RT	RT	220°C	Inkjet Printing
PM6:Y6 (1:1.2)	o-xylene + 5v% tetralin	3 mg/ml	60°C	RT	NA	Inkjet Printing
PM6:Y6 (1:1.2)	o-xylene + 5v% tetralin	3 mg/ml	60°C	RT	90°C	Inkjet Printing
PM6:Y6 (1:1.2)	o-xylene + 5v% tetralin	3 mg/ml	60°C	RT	165°C	Inkjet Printing
PM6:Y6 (1:1.2)	o-xylene + 5v% tetralin	3 mg/ml	60°C	RT	220°C	Inkjet Printing
PM6:Y6 (1:1.2)	o-xylene + 5v% tetralin	3 mg/ml	60°C	40°C	NA	Inkjet Printing
PM6:Y6 (1:1.2)	o-xylene + 5v% tetralin	8 mg/ml	RT	RT	165°C	Spin Coating
PM6:Y6 (1:1.2)	Chloroform	8 mg/ml	RT	RT	80°C	Spin Coating
PM6	o-xylene + 5v% tetralin	3 mg/ml	RT	RT	NA	Inkjet Printing
PM6	o-xylene + 5v% tetralin	3 mg/ml	60°C	RT	220°C	Inkjet Printing
Y6	o-xylene + 5v% tetralin	3 mg/ml	RT	RT	NA	Inkjet Printing
Y6	o-xylene + 5v% tetralin	3 mg/ml	RT	RT	220°C	Inkjet Printing

In **Figure 4** is shown the 1D linecuts of the diffraction patterns of neat films of PM6 and Y6 in the in-plane (IP) and out-of-plane (OOP) directions, measured at different temperatures while heating the samples in-situ. On the graph is also indicated the expected positions of the diffraction peaks representing lamellar stacking, amorphous regions, and π-π stacking. Both PM6 and Y6 films show a mixed face-on and edge-on orientation. The intensities of the peaks corresponding to the π-π stacking of PM6 increase with increasing temperature, suggesting enhanced crystallinity, whereas the opposite trend is observed in the case of Y6. Although amorphous peaks exist for thin films of both molecules, their intensities are very low.

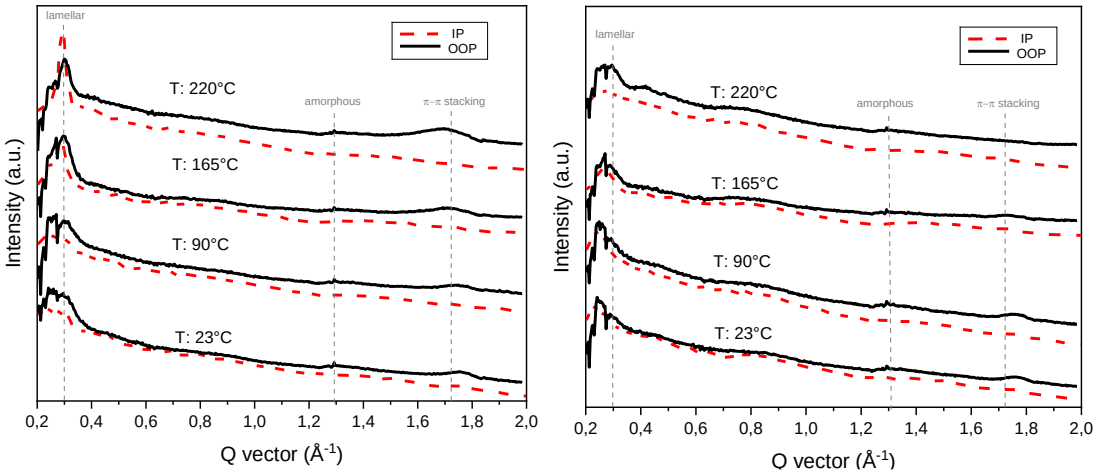

Figure 4. In-situ GIWAXS results of neat films of PM6 (left) and Y6 (right). The samples were prepared by ink-jet printing at room temperature without further thermal annealing.

For blend films of PM6 and Y6 inkjet-printed at plate temperatures of room temperature (RT) and 60°C, the 1D GIWAXS linecuts at different in-situ temperatures have been shown in **Figure 5**. The blend films show a mixed kind of orientation as well. The intensity of the amorphous peak decreases as the temperature increases, indicating the presence of more crystalline regions. This conclusion is also bolstered by the increased intensities of the peaks corresponding to lamellar stacking, and the merger of many lamellar stacking peaks at low temperatures into a single peak at high temperatures. No significant changes however are observed in the intensities of the π-π stacking peaks. In addition, when the sample is printed on a 60°C pre-heated substrate, the intensity of the amorphous peak is significantly increased. The results suggest that the amorphous phase of PM6:Y6 could be minimized by preparing samples at room temperature and following thermal annealing.

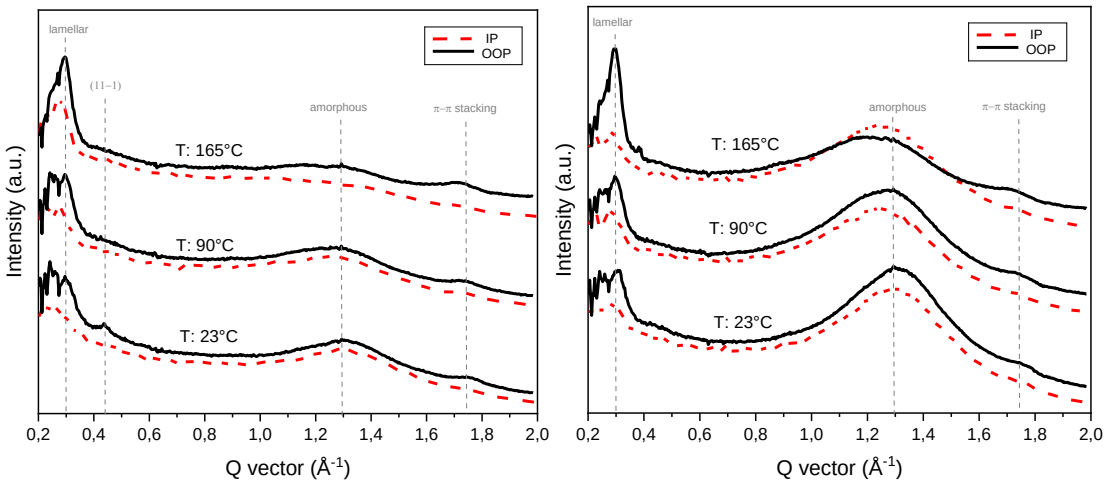

Figure 5. In-situ GIWAXS results of blend films inkjet-printed at RT (left) and 60°C (right)

The crystalline coherence lengths in the IP and OOP directions, calculated by the Scherrer equation, for the blend films measured in-situ are mentioned in **Table 2**. The general trend is that the CCL increases with increasing plate temperature. The results are less clear for annealing temperature, with increasing CCL with in-situ temperature in the IP direction and decreasing in the OOP direction. However, an exception to the trend is observed when increasing the in-situ temperature from 90°C to 165°C for the sample inkjet-printed at 60°C. In fact, this sample exhibits the highest observed IP CCL at 90°C. A possible cause for this observation might be temperature-induced degradation of the active layer.

Table 2: IP and OOP CCLs for PM6:Y6 films measured in-situ

Sample	IP CCL (Å)	OOP CCL (Å)
PM6:Y6 PT: 23°C, 23°C	8.36	11.10
PM6:Y6 PT: 23°C, 90°C	11.39	9.20
PM6:Y6 PT: 23°C, 165°C	11.56	9.11
PM6:Y6 PT: 60°C, 23°C	13.74	16.64
PM6:Y6 PT: 60°C, 90°C	21.88	14.56
PM6:Y6 PT: 60°C, 165°C	8.37	10.66

The results for the other samples, processed completely ex-situ and measured at room temperature, are shown in **Figure 6**. A number of conclusions can be drawn from these. Firstly, the film spin-coated from the solution of PM6:Y6 in o-xylene and tetralin shows a higher lamellar stacking peak and a similar π-π stacking peak in comparison with the one coated from a solution of chloroform. The difference in morphology may arise from the slower drying of the higher boiling-point xylene solvent compared to chloroform. This indicates that these more eco-friendly solvents might be used in place of chloroform without compromising, and even potentially enhancing, the crystallinity. Secondly, the spin-coated samples show no amorphous peaks while the inkjet-printed ones do. Therefore, further film optimization must be carried out in order to minimise amorphousness using inkjet-printing as the method of fabrication. Thirdly, increasing the thermal annealing temperature for blend films results in an increase in the intensity of the π-π stacking peak and merging of lamellar stacking peaks, indicating increased crystallinity. Fourthly, the blending process for PM6:Y6 might induce an extra structure which is labeled as the amorphous peak. Lastly, as observed for the in-situ annealed samples, increasing the plate temperature while printing tends to reduce the intensity of the amorphous peak.

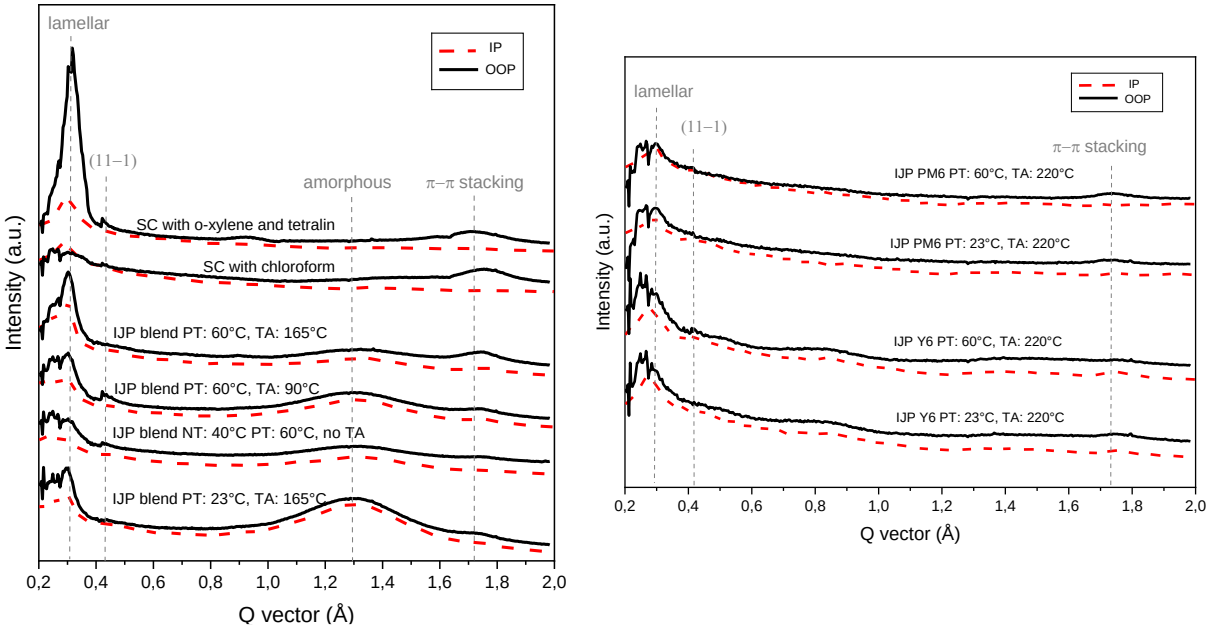

Figure 6. 1D GIWAXS linecuts for blend films (left) and neat films (right) processed ex-situ

Conclusion

During this beam time, the effects of additives and post-treatment on DIW-printed PEDOT:PSS pillars were investigated by WAXS. Among the additives, only Li salt was found to change the crystalline structure. According to the WAXS results, Li salt induces a new peak and shortens the PEDOT π-π stacking distance, which could be the main reason for the increased electrical conductivity. In contrast, GOPS induces no difference in WAXS results and seems independent of the thermoelectric performance of PEDOT:PSS pillars. In a nutshell, the WAXS result reveals the structural change from additives, and guides the way to optimize the thermoelectric performance of printed PEDOT:PSS by tuning Li salt content.

Results from the experiments conducted at ESRF allowed us to study the change in crystallinity of an OPV active layer (consisting of PM6 and Y6) with different processing conditions. It was found that the traditionally used but relatively toxic solvent chloroform could be replaced with greener alternatives such as o-xylene and tetralin, and this could in fact enhance the crystallinity. This opens doorways for applications of OPVs on smart wearables and biomedical devices, where biocompatibility and biotoxicity are important considerations. Inkjet-printing OPVs at higher temperatures generally improves crystallinity. In addition, increasing the thermal annealing or the in-situ temperature also leads to better crystallinity. This might be attributed to temperature-induced diffusion allowing for more movement and better packing of the molecules. However, caution must be exercised to ensure that the annealing temperature is not high enough to cause degradation.

Future work

For our OTEs project, the WAXS results provided sufficient understanding of how the additives change PEDOT crystalline structure and guided our formulation to boost thermoelectric performance. Alongside the previous WAXS results from experiments A26-2-945 and A26-2-952, the WAXS result from this experiment will be included in one of our manuscripts under preparation.

For our OPV project, attempts will be made to correlate the results from these experiments with OPV device performances. Doing so will help us shed light on the relationship between crystallinity,

morphology and performance, and determine the optimal conditions for processing OPVs for specific applications.

Reference

1. Untilova, V., Zeng, H., Durand, P., Herrmann, L., Leclerc, N., & Brinkmann, M. (2021). Intercalation and ordering of F6TCNNQ and F4Tcnq Dopants in regioregular poly(3-hexylthiophene) crystals: Impact on anisotropic thermoelectric properties of oriented thin films. *Macromolecules*, *54*(13), 6073–6084.
2. Saxena, N., Keilhofer, J., Maurya, A. K., Fortunato, G., Overbeck, J., & Müller-Buschbaum, P. (2018). Facile optimization of thermoelectric properties in Pedot:PSS thin films through Acido-base and redox Dedoping using readily available salts. *ACS Applied Energy Materials*, *1*(2), 336–342.
3. Huang, X., Deng, L., Liu, F., Liu, Z., & Chen, G. (2021). Aggregate structure evolution induced by annealing and subsequent solvent post-treatment for thermoelectric property enhancement of PEDOT:PSS Films. *Chemical Engineering Journal*, *417*, 129230.
4. Wang, Y., Zhu, C., Pfattner, R., Yan, H., Jin, L., Chen, S., Molina-Lopez, F., Lissel, F., Liu, J., Rabiah, N. I., Chen, Z., Chung, J. W., Linder, C., Toney, M. F., Murmann, B., & Bao, Z. (2017). A highly stretchable, transparent, and conductive polymer. *Science Advances*, *3*(3).
5. Ma, L.-K., Chen, Y., Chow, P. C. Y., Zhang, G., Huang, J., Ma, C., Zhang, J., Yin, H., Hong Cheung, A. M., Wong, K. S., So, S. K., & Yan, H. (2020). High-efficiency indoor organic photovoltaics with a band-aligned interlayer. *Joule*, *4*(7), 1607–1611.